



Vortex shedding patterns in flow past a streamwise oscillating square cylinder at low Reynolds number using dynamic meshing

Cite as: Phys. Fluids **31**, 113605 (2019); <https://doi.org/10.1063/1.5123347>

Submitted: 06 August 2019 . Accepted: 28 October 2019 . Published Online: 18 November 2019

Harshal S. Raut , and Harish N. Dixit 



View Online



Export Citation



CrossMark

ARTICLES YOU MAY BE INTERESTED IN

[Three-dimensional simulation of tracer transport dynamics in formations with high-permeability channels or fractures: Estimation of oil saturation](#)

Physics of Fluids **31**, 113604 (2019); <https://doi.org/10.1063/1.5120415>

[Vortex-induced vibration and galloping of a circular cylinder in presence of cross-flow thermal buoyancy](#)


Physics of Fluids **31**, 113603 (2019); <https://doi.org/10.1063/1.5122851>


[Space-time correlations of velocity in a Mach 0.9 turbulent round jet](#)

Physics of Fluids **31**, 115108 (2019); <https://doi.org/10.1063/1.5128424>



CAPTURE WHAT'S POSSIBLE
WITH OUR NEW PUBLISHING ACADEMY RESOURCES

Learn more 



Vortex shedding patterns in flow past a streamwise oscillating square cylinder at low Reynolds number using dynamic meshing

Cite as: Phys. Fluids 31, 113605 (2019); doi: 10.1063/1.5123347

Submitted: 6 August 2019 • Accepted: 28 October 2019 •

Published Online: 18 November 2019



View Online



Export Citation



CrossMark

Harshal S. Raut¹  and Harish N. Dixit^{2,a)} 

AFFILIATIONS

¹Indian Institute of Technology Bombay, Powai, Mumbai 400076, India

²Indian Institute of Technology Hyderabad, Kandi, Sangareddy 502285, India

^{a)}Electronic mail: hdixit@iith.ac.in

ABSTRACT

We present a two-dimensional numerical study for uniform flow past a streamwise oscillating square cylinder at a Reynolds number of 200. To overcome the limitations with an oscillating inlet flow as used in earlier studies, a dynamic meshing feature is used to oscillate the cylinder. A parametric study is carried out by varying amplitude and frequency of cylinder oscillation. Two symmetric modes, named here as S-II-I and S-IV-D, have been found. In S-II-I mode, a pair of vortices are shed symmetrically on each side of the cylinder in one cycle (S-II mode), and in S-IV-D mode, two pairs of vortices of opposite sense are shed on each side of the cylinder. A vortex flapping mode has also been obtained for low to moderate amplitude and frequency ratios. A new mode of vortex shedding termed the “vortex dipole” mode is found and involves the alternate arrangement of vortex pairs unlike the zigzag arrangement of single vortices in a Kármán vortex street. As in most nonlinear oscillators, vortex shedding becomes chaotic when forced sufficiently strongly and is usually associated with nonlinear interactions between competing frequencies. Many modes observed in the current study become chaotic when the peak cylinder velocity becomes comparable with the inlet velocity. The 0-1 test for chaos is applied to the time series of lift coefficient to show that the signals are truly chaotic. We also observe chaos due to mode competition when shedding transitions from an antisymmetric to symmetric modes.

Published under license by AIP Publishing. <https://doi.org/10.1063/1.5123347>

I. INTRODUCTION

The study of vortex-induced vibrations (VIVs) is an area of active research with many open questions of fundamental and applied nature. Vibrations of pipes in heat exchangers and civil engineering structures due to hydrodynamic loads have been extensively studied. Structural failure may result from synchronization between the fluid excitation force and natural frequency of the system. This hydrodynamic load can sometimes lead to motion of the structure in the streamwise direction.^{19,30} The problem of streamwise oscillation could be particularly severe when a lightly damped cylindrical structure is used in liquids of high density such as water, oil, and metal at high temperatures.

It is known that flow past stationary bluff bodies leads to anti-symmetric vortex shedding behind the body called the Kármán vortex street. In this case, the vortices arrange themselves in a zigzag

pattern of alternating strength. A large number of studies have focused on transverse oscillations of cylinders^{6,15,33} primarily due to interest in understanding vortex-induced vibrations (e.g., Williamson and Govardhan⁴⁰ and references therein). Other recent studies involving wakes due to vortex shedding from cylinders include the effect of rotational motion of a circular²⁵ and elliptical² cylinder, wake flow subjected to free surface wave excitations,²⁷ transverse oscillations of triangular cylinders,¹ and an inline oscillating cylinder in tandem with a stationary cylinder⁴² to name a few.

The focus of the present study is to shed light on various shedding patterns found in an inline oscillating square cylinder. It has been observed in experiments^{4,9,22,31,41} that inline oscillations of the body can lead to a variety of antisymmetric, symmetric, or even chaotic modes of vortex shedding. Symmetric modes of shedding have also been observed in numerical simulations,^{21,23,24,35,43} but to

the best of our knowledge, all simulations rely on using an oscillating inlet with a stationary body rather than oscillate the body. Pioneering flow visualization studies were carried out by Tatsuno and Bearman³⁶ for flow induced by an oscillating circular cylinder in a quiescent fluid. The Keulegan-Carpenter (KC) and Stokes (β) numbers were varied in the range of 1.6–15 and 5–160, respectively. A number of fascinating flow patterns were observed, including symmetric, oblique, and antisymmetric vortex shedding. Direct numerical simulations (DNS) and Floquet analysis by Elston *et al.*^{11,12} reveals that the visual patterns observed in Tatsuno and Bearman can be explained with a two-dimensional analysis. This also suggests that the three-dimensionality for a majority of the modes in the above range of KC and β is weak in the case of an oscillating circular cylinder.

The above studies do not have a net mean flow. Adding a net mean flow introduces a new frequency into the problem, f_o , which is the natural vortex shedding frequency for flow past a stationary cylinder. Though a direct comparison of the present study with Tatsuno and Bearman³⁶ or Elston *et al.*¹² is difficult, a qualitative comparison has been carried out. All results presented in this paper are given in terms of nondimensional amplitude, A/h , and frequency ratio, f_e/f_o , as was used in some earlier studies.^{21,28,35} The results can be easily expressed in terms of KC and β through the following simple relations:

$$KC = 2\pi\left(\frac{A}{h}\right), \quad \beta = \frac{f_e d^2}{\nu} = \left(\frac{f_e}{f_o}\right) St Re, \quad (1)$$

where $St = f_o h/U_m$ and $Re = U_m h/\nu$ are the Strouhal and Reynolds numbers, respectively, for a stationary cylinder with a constant inlet flow, U_m . Among the various studies done on flow past inline oscillating circular cylinder, Griffin and Ramberg¹⁹ were among the first to carry out a systematic experimental study. They found a *lock-on* regime in the range of $1.2 < f_e/f_o < 2.5$, where the vortex shedding frequency matches the excitation frequency. The presence of lock-on provides an interesting avenue for flow control as was discussed in the review of Griffin and Hall.¹⁸ Minewitsch *et al.*²⁸ carried out a systematic numerical study by varying both amplitude and frequency of excitation to study the lock-on regime in detail. All their computations were carried out at $Re = 200$ for a square cylinder with an oscillating inlet. They generate a phase diagram in the frequency-amplitude plane and show that the lock-on regime is sandwiched below the region-of-superposition where combination frequencies arise. No symmetric, flapping, or chaotic modes were observed in their study. Ongoren and Rockwell³¹ in the second of a two part paper on vortex formation behind cylinders of various cross section discussed their experiments on a cylinder oscillating at an angle α , where $0^\circ \leq \alpha \leq 90^\circ$, relative to the incoming flow. Various flow structures were classified based on symmetry, vortex arrangement, etc. In brief, they observed one symmetric (called S-I) and four antisymmetric wake patterns behind the circular cylinder. Konstantinidis and Balabani²² in their experimental study also noted the S-I mode wherein a pair of vortices of opposite sign are simultaneously shed on either side of the cylinder. Xu *et al.*⁴¹ performed experimental studies and discovered a new mode of symmetric shedding called S-II, where two pairs of vortices, vortex dipoles, are shed from each side of the cylinder, but in their case, they were not able to obtain a fully symmetric S-II mode as the symmetric vortices got distorted

downstream. They erroneously conclude that the new mode can be explained as a simple superposition of symmetric and antisymmetric modes. The origin of error lies in an algebraic error in their derivation of the vorticity equation. The S-II mode has also been obtained by Krishnan *et al.*^{24,23} in their numerical studies on flow past an inline oscillating square cylinder, but they were also not able to obtain a fully symmetric S-II mode that can be attributed to the range of parameters that they considered, using an oscillating inlet flow or different Reynolds number. Krishnan *et al.*²⁴ found that in the mechanism of formation of several vortex shedding modes, the interaction of base region vortices with the main shear layer vortices plays an important role. In a further study, Krishnan *et al.*²³ correlated the characteristics of the force coefficients to the near body vortical events and also looked into the feasibility of energy extraction from the flow. Lecoite and Piquet²⁶ carried out numerical simulations of flow past inline and transversely oscillating cylinders. They reported a single symmetric mode, S-I, and their study was restricted to low amplitude and frequency ratios. Feymark *et al.*¹³ carried out experimental and large eddy simulations for flow past stationary and inline oscillating circular cylinders. Their experimental study was carried out for fixed amplitude ratio, $A/h = 0.96$, and a wide range of Reynolds numbers, $405 \leq Re \leq 2482$. Their LES study was restricted to a fixed frequency ratio, $f_e/f_o = 1$, and was found to be in agreement with their experiments, especially the presence of lock-on states.

Apart from symmetric and antisymmetric shedding, chaotic vortex shedding was reported by Vittori and Blondeaux³⁸ and Perdikaris *et al.*³² The former study had no mean flow and showed that the route to chaos is quasiperiodic, whereas the latter study suggested that mode competition led to chaos. Srikanth *et al.*³⁵ noted that chaos occurs when the flow transitions from an asymmetric shedding to a symmetric shedding with either change in frequency or amplitude of oscillation. A similar result has also been found in the present study. Following the work of Gottwald and Melbourne,^{16,17} a rigorous 0-1 test for chaos is applied on the time series of lift coefficient to show that a periodic signal corresponding to an antisymmetric shedding becomes chaotic with increase in amplitude of cylinder oscillation and eventually leads to symmetric shedding on further increase in amplitude. This clearly established the mode-competition route to chaos alluded to in previous studies.^{32,35}

Though all experiments reported above deal with a cylinder oscillating in a constant inlet flow, numerical challenges associated with moving a cylinder have restricted almost all numerical studies to the case of stationary cylinders with an oscillating inlet. If the inlet velocity is modulated in a periodic fashion, then it is essential that the minimum velocity in a given period is kept positive to preserve the nature of the inlet and outlet boundary conditions. Consider an inlet with an oscillating velocity²⁸ given by

$$U_i = U_m + \Delta U \cos(\omega t),$$

where U_i , U_m , and ΔU are the magnitudes of the total, mean, and fluctuating velocities at the inlet, respectively, and ω is the frequency of pulsation. To preserve the nature of the boundary condition at the inlet and outlet, we require that $\Delta U \leq U_m$. This restricts the range of fluctuating velocities that can be studied in such computations. To overcome this difficulty, we have chosen to carry out simulations with a cylinder oscillating in a uniform inlet. This is perhaps

the first systematic study for inline oscillating cylinders where the cylinder is in motion. We use the open-source computational fluid dynamics (CFD) code *OpenFOAM*³⁹ with the dynamic meshing feature for all computations reported here. To simplify the complexity in mesh generation and mesh motion, we use a square cylinder for the present study. Nevertheless, we expect the results presented in this paper to be valid for cylinders of other shapes. Alternately, it is also possible to use vortex blob methods⁷ for such computations, but the ease of usage and excellent functionality of *OpenFOAM*³⁹ prompted us to use the latter. In a recent study, Lee²⁷ used *OpenFOAM* to study the response of the wake to wave excitation arising from a free surface.

For all simulations reported in this paper, we keep the Reynolds number based on the mean velocity fixed at 200 since this value has been used in other studies too.^{28,35} Emphasis will be given to parameter regimes not previously investigated, so a discussion on lock-on regime is largely omitted from the paper. The analysis is also restricted to two dimensions. As noted by Elston *et al.*,¹² flow field due to an oscillating cylinder is largely two-dimensional in nature. We assume that this two-dimensional nature is not significantly altered due to a mean flow. Nabatian *et al.*²⁹ performed three-dimensional (3D) numerical simulations for flow past inline oscillating square cylinder in which they kept the frequency of oscillation constant at natural vortex shedding at Reynolds number of 200 and varied amplitude ratio up to 0.5 and found that the 3D spanwise effect is suppressed at Reynolds number of 200 by streamwise oscillation of the cylinder and that two-dimensional (2D) simulations can effectively model the temporal instability of wake flow. This is similar to the findings of Toebes³⁷ who found that transverse oscillations of cylinder increase spanwise correlations of velocities and forces, thus giving the flow a characteristically two-dimensional nature even at higher Reynolds number. This was indeed the reason cited by Blackburn and Henderson⁵ to perform two-dimensional simulations even at Reynolds number as high as 500.

We acknowledge that three-dimensional effects may appear even at the lower value of $Re = 200$ used in the present study, but we assume that three-dimensionality does not completely destroy the two-dimensional modes found here. For higher amplitude or frequency values where the fluctuating velocity, ΔU , can be high, our simulations may be susceptible to three-dimensional effects. Full 3D simulations are computationally expensive and is currently beyond the scope of the present study. It should also be noted that two-dimensional experiments with thin films can be carried out as was done in the experiments of Couder and Basdevant⁸ who studied vortex streets due to an inline oscillating cylinder in a flowing soap film. Similar experiments can be carried out for the parameter range considered in the present paper to verify the veracity of the results observed in the present study.

The main goal of this paper is to highlight the effect of amplitude and frequency ratio on vortex shedding characteristics along with a careful characterization of chaotic modes. We have therefore carried out an extensive parametric study involving more than 100 simulations varying the amplitude of the cylinder motion and its frequency. Two new shedding modes are discovered, namely, the S-IV-D mode and the vortex dipole mode. A stable S-II mode (here referred to as S-II-I) is obtained for the first time in this study. This mode was recently discovered but was found to be unstable to anti-symmetric perturbations. All results are summarized in the form of

a “phase diagram” in the amplitude-frequency plane where parameter ranges for various modes are delineated. In addition, chaotic modes are tested by 0-1 test of chaos. Another important novelty of the paper as discussed above is the use of dynamic moving mesh rather than have the cylinder oscillate. The advantage of using such a feature is discussed in detail in Sec. II.

The rest of the paper is organized as follows: Section II discusses the problem formulation, the dynamic meshing approach employed for the simulations, and a validation of the code with existing literature. A detailed study of various modes obtained by varying the amplitude and frequency of excitation is discussed in Sec. III. Chaotic vortex shedding and its characterization are contained in Sec. IV. We briefly contrast and compare the present study with the study of Tatsuno and Bearman³⁶ for a circular cylinder in a quiescent flow in Sec. V. Section VI concludes the paper along with a brief discussion on future outlooks.

II. FORMULATION, NUMERICAL APPROACH, AND VALIDATION

In the present study, incompressible Navier-Stokes equations are solved with no-slip boundary condition on the surface of the square cylinder. The velocity is uniform at the inlet (i.e., left of computational domain), Neumann boundary conditions are used at the outlet, and free slip boundary conditions are employed at the top and bottom of the computational domain.

All numerical simulations have been performed in *OpenFOAM* v2.3.0, a free open source CFD software³⁹ containing a variety of solvers for different flow applications. The solver used for the present simulations is *pimpleDyMFoam*, which is an extension of the *pimpleFoam* solver for dynamic meshes. The solver is transient, allows for relatively large time steps, and uses a hybrid PISO-SIMPLE algorithm called the PIMPLE algorithm. The standard Gaussian finite volume integration has been chosen for discretization. Gaussian integration is based on summing values on cell faces, which must be interpolated from cell centers. For diffusion terms in Navier-Stokes equations, linear interpolation is used for interpolation of kinematic viscosity and limited scheme (blend of corrected and uncorrected) is used to compute the surface normal gradient at the cell faces. For convection terms, the linearUpwind scheme is used as the interpolation scheme. For all simulations, the Courant number is restricted to 0.5 and an adaptive time stepping scheme is employed.

The dynamicMotionSolverFvMesh function has been used to perform mesh motion without topological changes following Laplace’s equation for motion displacement (d_m) given by

$$\nabla \cdot (\gamma \nabla d_m) = 0, \quad (2)$$

where γ is the mesh diffusivity parameter. Tuning the parameter γ restricts the region over which the mesh deforms as the cylinder oscillates. In the current study, we have used displacementLaplacian as the solver and a quadratic diffusivity model to calculate the diffusion coefficient.

To study the effect of inline oscillations, we prescribe a harmonic motion for the cylinder, $x_b(t)$, in the direction of the incoming flow as

$$x_b(t) = x_0 + A \sin(\omega t), \quad (3)$$

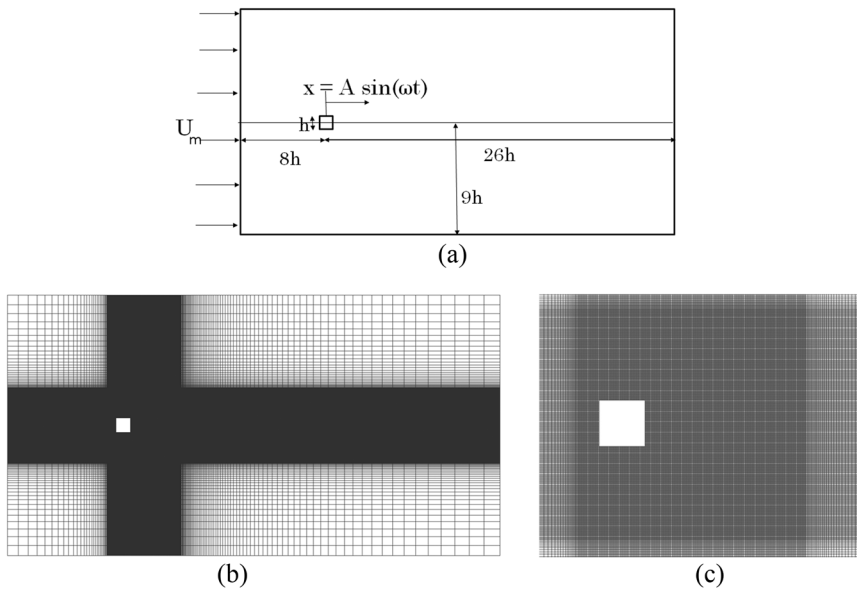


FIG. 1. (a) Schematic of the domain used in the simulations along with its dimensions, (b) the grid at the beginning of the simulation [dimensions same as in (a)], (c) high-density grid in the vicinity of the cylinder within a square of size $5h \times 5h$ with $(-h, -2.5h)$, $(4h, -2.5h)$, $(-h, 2.5h)$, and $(4h, 2.5h)$ as the corners of the square.

where x_0 is the mean position of the cylinder, A is the amplitude, and $\omega = 2\pi f_e$ is the circular frequency of motion. Differentiating the above equation with time, the velocity of the cylinder, $U_b(t)$, in the direction of the flow is given by

$$U_b(t) = A\omega \cos(\omega t). \tag{4}$$

At the inlet, we prescribed a constant uniform flow, U_m . For $A\omega < U_m$, the maximum cylinder velocity is less than the inlet flow and relative velocity between incoming flow and cylinder is expected to be positive at all times, whereas for $A\omega > U_m$, for a certain duration of each period, the net relative velocity between the incoming flow and cylinder is negative; i.e., the cylinder is moving counter to the incoming flow in absolute sense. This regime cannot be simulated in the usual way with a stationary cylinder and an oscillating inlet since prescribing a negative velocity at the inlet leads to numerical complications. The present study is the first numerical study to investigate this regime.

The nondimensional parameters involved in our simulations are Reynolds number (Re), aspect ratio of the cylinder which is the ratio of height of the cylinder to that of the width of the cylinder, frequency ratio which is the ratio of forcing frequency of oscillating cylinder to that of vortex shedding frequency of stationary cylinders at the same Reynolds number (f_e/f_o), and amplitude ratio which is the ratio of amplitude of oscillating cylinder to that of the height of the cylinder (A/h). In our simulations, we have kept the Reynolds number constant at 200 and aspect ratio at 1. The f_o value obtained from our simulation for stationary cylinder at Reynolds of 200 was 0.152 04. This matches the Strouhal number value given by Okajima³⁰ for a square cylinder at Reynolds number of 200 (with $h = 1$ and $U_m = 1$ that we used in our simulations).

Figure 1(a) shows the domain used for the simulations; h stands for the height of the cylinder and all dimensions are characterized in terms of h . The size of the domain is $34h \times 18h$ with nonuniform grids of up to nearly 150 000 grid points, whose arrangement is

shown in Fig. 1(b). To capture the velocity gradients accurately for precise quantification of drag and lift forces, we use a high-density uniform grid in the vicinity of the cylinder as shown in Fig. 1(c) within a square of size $5h \times 5h$ with $(-h, -2.5h)$, $(4h, -2.5h)$, $(-h, 2.5h)$, and $(4h, 2.5h)$ as the corners of the square.

The domain size in Fig. 1(a) and the optimal values for grid points in the domain were obtained after extensive validation studies and comparison with existing numerical results for a stationary cylinder. A sample of the key studies is given in Tables I–IV, which shows the results of the grid and domain dependence studies done for $f_e/f_o = 1.5$, $A/h = 0.05$, and $Re = 200$. For grid dependence, the total number of grid points were increased by a factor of 1.67, which resulted in variation in grid points on each face of the cylinder, N_s , from 60 to 100. For domain dependence, we separately vary the vertical domain size, H , to study the effect of blockage ratio, Table II, and the effect of downstream distance from the cylinder to the outlet boundary, Table III, and the effect of upstream distance from the cylinder to the inlet boundary, Table IV. In these tables, f_1 and f_2 indicate the frequencies obtained from the spectra of lift coefficient, $C_{D,mean}$ and $C_{L,rms}$ stand for the mean drag coefficient and root-mean-square value of lift coefficient, respectively. The maximum deviation in the above parameters is well within acceptable limits. Based on these studies, a mesh with $N_s = 60$ points on each side of the cylinder and a grid size of 409×370 are chosen for all subsequent simulations.

TABLE I. Details of the grid dependence test with domain size as shown in Fig. 1(a).

Grid size	N_s	f_1	f_2	$C_{D,mean}$	$C_{L,rms}$
409×370	60	7.573×10^{-2}	0.151 75	7.763×10^{-2}	2.652×10^{-2}
618×682	100	7.263×10^{-2}	0.154 06	7.706×10^{-2}	2.532×10^{-2}

TABLE II. Details of the domain dependence test for blockage.

Blockage (%)	Grid size	f_1	f_2	$C_{D,mean}$	$C_{L,rms}$
5.56 (H = 18)	409 × 370	7.573×10^{-2}	0.151 75	7.763×10^{-2}	2.652×10^{-2}
4.16 (H = 30)	409 × 436	7.520×10^{-2}	0.150 46	7.733×10^{-2}	2.648×10^{-2}

TABLE III. Details of the domain dependence test for downstream distance.

Downstream distance	Grid size	f_1	f_2	$C_{D,mean}$	$C_{L,rms}$
26h	409 × 370	7.573×10^{-2}	0.151 75	7.763×10^{-2}	2.652×10^{-2}
56h	497 × 370	7.475×10^{-2}	0.149 10	7.559×10^{-2}	2.502×10^{-2}

TABLE IV. Details of the domain dependence test for upstream distance.

Upstream distance	Grid size	f_1	f_2	$C_{D,mean}$	$C_{L,rms}$
8h	409 × 370	7.573×10^{-2}	0.151 75	7.763×10^{-2}	2.652×10^{-2}
14h	497 × 370	7.527×10^{-2}	0.150 55	7.572×10^{-2}	2.492×10^{-2}

The numerical approach was validated as follows: For the Reynolds numbers relevant to the present study, Strouhal numbers obtained from flow past a fixed square cylinder were found to be in good agreement with the experiments of Okajima,³⁰ numerical simulations of Ansumali *et al.*,³ and Sohankar *et al.*³⁴ We also validated our result with Minewitsch *et al.*²⁸ by comparing the power spectrum of lift coefficient at $A/h = 0.25$ and $f_e/f_o = 2$, as shown in Fig. 2. For future reference, in all plots showing the spectrum of lift coefficient, the vertical line (---) represents f_e and (---) represents f_o . The lock-on window observed by Minewitsch *et al.*²⁸ for a fixed amplitude ratio of $A/h = 0.225$ was also observed in the present

simulations as shown in Fig. 3, where f_v is the actual frequency of vortex shedding which is found to be equal to $0.5f_e$ in the lock-on window.

We further validate the numerical code by reproducing the S-II mode obtained by Khaledi *et al.*²¹ for flow past an oscillating plate of aspect ratio of 50. As shown in Fig. 4, there is an excellent comparison in the vorticity plots. The direction of vorticity vector in Khaledi *et al.* is opposite to that used in this paper; hence, the colors are opposite to each other. Despite the larger domain used in Khaledi *et al.*, the vorticity plots agree quite well. Because of a moving grid employed in the present simulations, we use a slightly coarser mesh

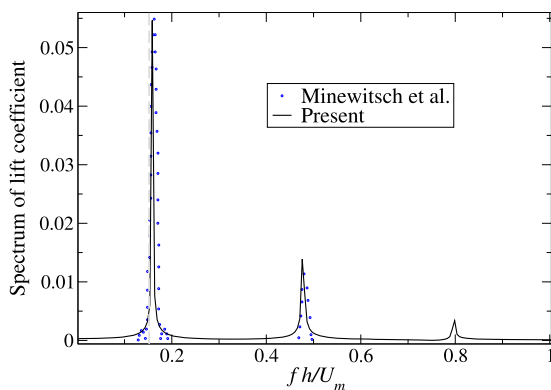


FIG. 2. Comparison of power spectra of lift coefficient from Minewitsch *et al.*²⁸ with our results at $A/h = 0.25$ and $f_e/f_o = 2$.

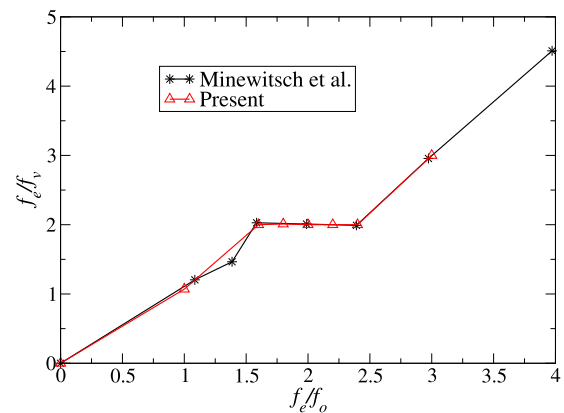


FIG. 3. Comparison of lock-on phenomenon with data given in Minewitsch *et al.*²⁸ for $A/h = 0.225$ and $1 < f_e/f_o < 3$.

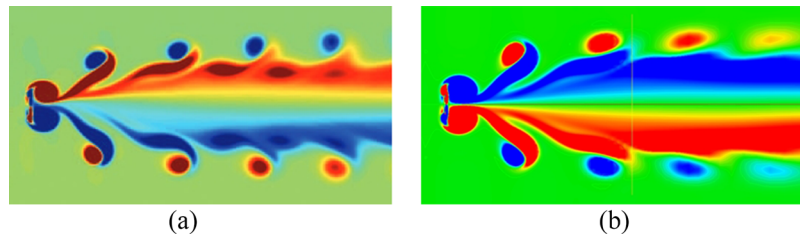


FIG. 4. Comparison of vorticity contours for the S-II mode from Khaledi *et al.*²¹ (a) with our result (b) for $A/h = 0.5$, $f_e/f_o = 1.74$ and $Re = 100$ at the same phase. In our case, the cylinder center is at a distance of $8h$ from the inlet. The two figures are to the same scale and employ same color bar ranging from -1 to $+1$. The opposite colors in the two plots are due to opposite sign convention in the definition of vorticity. Figure 4(a) reproduced with permission from Khaledi *et al.*, “Flow past a normal flat plate undergoing inline oscillations,” *Phys. Fluids* **24**, 093603 (2012). Copyright 2012 AIP Publishing LLC.

than Khaledi *et al.* The difference in the sharpness of the two images could therefore be attributed to differing grid densities in the two studies.

III. MODE CHARACTERISTICS

An extensive parametric study ranging over 100 simulations has been performed by systematically varying the amplitude ratio, A/h , and frequency ratio, f_e/f_o . All simulations are carried out with a Reynolds number based on the constant inlet velocity, U_m , fixed at 200. A summary of all simulations is shown in the form of a “phase diagram” in Fig. 5. Neat clusters of similar shedding modes are clearly visible in the plot. It can be observed that the symmetric modes are obtained at both high amplitude-low frequency and high frequency-low amplitude regions. The vortex flapping modes, to be discussed later, are obtained for frequency ratio between 0.8 and 1.5. At low amplitude ratios, beyond $f_e/f_o > 3$, the modes appear to become progressively symmetric with increasing amplitude ratio and for $f_e/f_o > 4.25$, a symmetric mode, S-IV-A, is observed. We find

that the shedding becomes chaotic as we move close to the line where the peak body velocity, $A\omega$, becomes equal to the inlet velocity, U_m . Recall that $\omega = 2\pi f_e$; thus, we have

$$2\pi f_e A = U_m \implies \left(\frac{A}{h}\right)\left(\frac{f_e}{f_o}\right) = \frac{U_m}{2\pi h f_o}, \quad (5)$$

which is the equation of a rectangular hyperbola as shown in Fig. 5. Chaotic vortex shedding is also observed during mode transition from antisymmetric to symmetric mode at low frequencies with the increase in amplitude ratio. Unlike earlier studies, a rigorous test for chaos is employed on the time series of lift coefficient and is discussed in Sec. IV. All results reported in this paper are in terms of f_e/f_o and A/h since this has been the common choice of parameters in many earlier works.^{19,21,28,35} But for a cylinder oscillating in a quiescent flow, a more convenient choice of parameters is KC and β as was used in Tatsuno and Bearman and Elston *et al.* The two set of parameters are directly related to each other with a simple scaling factor as given in Eq. (1). For convenience of the reader, we include these scalings in Fig. 5.

We now present a detailed discussion on the structure and characteristics of various modes of vortex shedding obtained. It has to be emphasized here that mode classification is based on the vorticity plots rather than streamline plots. Minewitsch *et al.* showed that for a time periodic flow, streamline plots for the same mode appear different at different instants of time within a period of oscillation. But we find that the vorticity plots for a given mode do not change their characteristic as can be seen from the movies attached in the supplementary material. Simulations were run up to a time of 300 s, and in almost all cases, transients persisted for about 50–70 s. All spectral analyses were carried out only after removing these initial transients.

A. Symmetric mode-I (S-II-I)

Two symmetric modes have been observed in our simulations. The first symmetric mode represented by the symbol (blue asterisk) in Fig. 5 is obtained for $f_e/f_o \approx 1$ and moderate values of A/h , or equivalently for $KC > 3$ and $\beta \approx 25$. The vorticity contours at a particular time and frequency ratio of $f_e/f_o = 0.807$ are shown in Fig. 6 for different amplitude ratios. We choose to classify the modes according to the vorticity plots since streamline plots can lead to misleading classification as shown by Minewitsch.²⁸

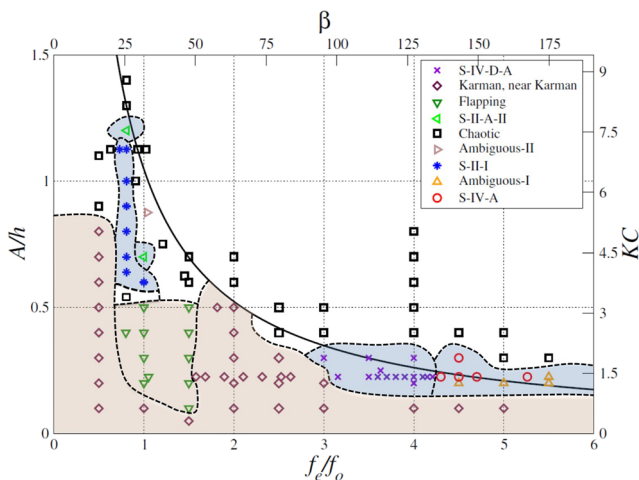


FIG. 5. A map of various shedding modes obtained by varying frequency, f_e , and amplitude, A , of excitation. The solid line is a rectangular hyperbola obtained by equating the inlet velocity with the peak velocity of the body, i.e., $A\omega = U_\infty$. See text for a detailed discussion on various modes and their nomenclature.

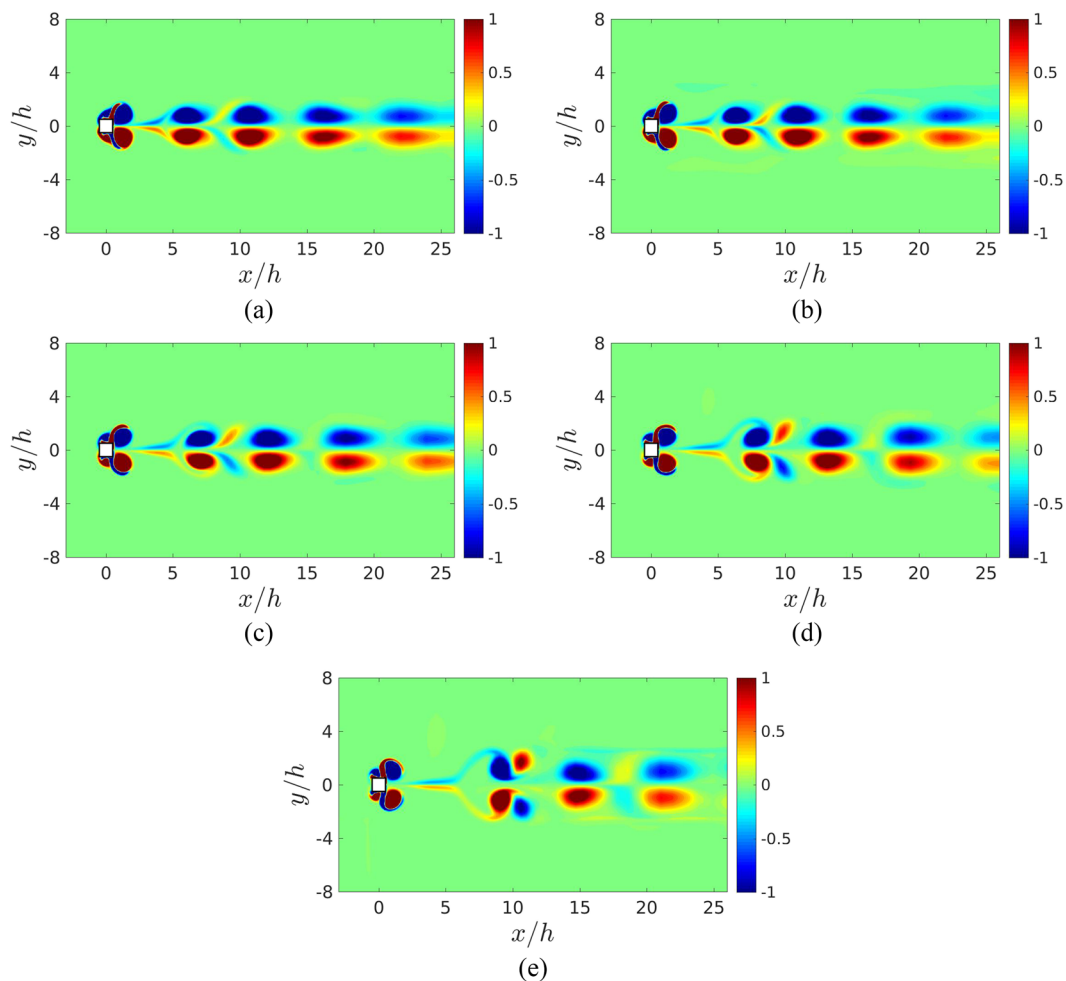


FIG. 6. Symmetric mode (S-II-I) obtained at $f_e/f_o = 0.807$ and (a) $A/h = 0.7$, (b) $A/h = 0.8$, (c) $A/h = 0.9$, (d) $A/h = 1$, (e) $A/h = 1.125$. In all cases, the cylinder center is at a distance of $8h$ from the inlet. (Color bars indicate vorticity in the z -direction in units of $1/s$.)

This mode is similar to the S-II mode reported earlier by Xu *et al.*⁴¹ and Krishnan *et al.*,^{24,23} but none of them were able to obtain a stable symmetric mode that is symmetric and identifiable throughout the domain which can be attributed to the different amplitude and frequency ratios, Reynolds number, shape of the cylinder (in the case of Xu *et al.*⁴¹), and the use of oscillating inlet (in the case of Krishnan *et al.*^{24,23}). This mode is also similar to the S-II mode obtained by Srikanth *et al.*³⁵ in the sense that that two vortices of opposite sense are shed from each side of the cylinder, but the structure of the mode is different in appearance from that reported by them. A pair of primary vortices of opposite sign start to form behind the cylinder as the cylinder moves against the flow. And when the cylinder moves with the flow, another small pair of secondary vortices are created. The primary and secondary vortices form a vortex pair, with the former dominating in strength. As the cylinder reaches its extremum point while moving with the flow, both the vortex pairs detach from the cylinder and form a pair of symmetric dipoles on each side of the centerline, creating the S-II mode. The entire

evolution of the mode in one shedding cycle can be found in the [supplementary material](#). Since the secondary vortex is weak, it gets sheared away as the vortices travel downstream, and thus, only the primary vortices on each side of the centerline survive, resulting in an S-I mode. We therefore name the combined vortex structures as S-II-I to indicate that two symmetric vortex pairs are shed from the cylinder, but a single symmetric pair survives as the structure travels downstream. A movie attached in the [supplementary material](#) shows the evolution of vorticity contours over a few oscillation cycles.

The parameters at which this mode appears in the present study was not studied in earlier numerical studies of either Srikanth *et al.*³⁵ (restricted to low A/h cases from 0.1 to 0.175) or Minewitsch *et al.*²⁸ (restricted to $A/h < 0.4$). This mode seems similar to that obtained by Zhou and Graham⁴³ for $Re = 600$, $KC = 3$, and $\beta = 200$ (Zhou and Graham report their results in terms of $B = U_m/2\pi f_e A = 1$), but their symmetric mode quickly switched to a Kármán-type alternating vortex street downstream of the cylinder. Even the pure

S-I mode reported in Zhou and Graham for $Re = 400$, $KC = 2$, and $\beta = 200$ also switched to an antisymmetric pattern downstream. This was attributed to a natural instability of the instability modes. But we report no such instability, and the observed S-II-I modes remain stable for a time much larger than that reported in Zhou and Graham. A number of differences are present between the two simulations—body shape, Reynolds number, the exact values of KC and β at which the symmetric modes were found in the two studies, and the differing numerical approaches in the two studies.

In the present study, the S-II-I mode is formed in a narrow band of frequency ratios and a wider band of amplitude ratios. As is evident from Fig. 6, the strength of the secondary vortices increases with increasing amplitude. The frequency of vortex shedding is found to be equal to f_e , i.e., $f_v = f_e$. Since the spacing between the successive vortex pairs is proportional to the “effective” flow velocity and inversely proportional to the frequency of shedding, we expect $l \propto U_{eff}/f_v$, and we can assume $U_{eff} = U_m + \alpha A\omega$ is the effective upstream velocity over one cycle of cylinder motion written in terms of the mean velocity, U_m , at the inlet and a fraction ($0 < \alpha < 1$) of the peak cylinder velocity, $A\omega$. With β as the proportionality constant and using $f_v = f_e$, we get

$$l = \frac{\beta(U_m + \alpha A\omega)}{f_e}. \quad (6)$$

The above relation shows that the vortex spacing depends linearly on the amplitude of cylinder motion. In the above expression, α and β can be determined by fitting measured vortex spacing against amplitude ratio, A/h . We measure the spacing between the S-I pair of vortices downstream of the cylinder in Fig. 6 and fit a straight line of the form $l = aA + b$ with $a = 2.324$ and $b = 3.703$. This is a least squares fit and approximates the data reasonably well as shown in Fig. 7. Comparing the fit to Eq. (6), we find $\alpha = 0.814$ and $\beta = 0.454$, suggesting that this mode of vortex shedding occurs when the peak cylinder velocity during oscillation is nearly 81% of the mean inlet velocity.

B. Symmetric mode-II (S-IV-D)

The second symmetric mode, represented by the symbol (red open circle) in Fig. 5, is found in the opposite end of the parameter space, i.e., for large f_e/f_o and small A/h . Vorticity plots for two such modes are shown in Fig. 8. This mode has again not been reported in earlier studies, especially the work of Srikanth *et al.*³⁵ and Minewitsch *et al.*,²⁸ as their study was restricted to $f_e/f_o < 4$. Moreover, this mode occurs in the vicinity of the hyperbola in Fig. 5

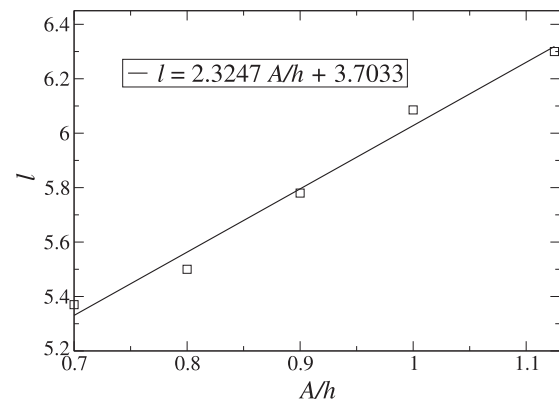


FIG. 7. Effect of amplitude ratio, A/h , on the spacing between the vortices, l , measured downstream of the cylinder for the S-II-I mode shown in Fig. 6 at frequency ratio $f_e/f_o = 0.807$.

where $A\omega$ is close to inlet velocity, which is difficult to achieve with an oscillating inlet simulation as opposed to a cylinder oscillating in a uniform flow.

In this mode, two pairs of vortices of opposite sense are being produced on each side of the cylinder across the centerline in one cycle. As the cylinder moves against the incoming flow, a vortex pair on the front and rear side of the cylinder forms symmetrically on the top and bottom side, and as the cylinder recedes in the direction of incoming flow, one vortex out of each vortex pair grows, rolls up, and moves away, while the other spreads out. As a result, there are two vortex pairs shed from each side (top and bottom) of the cylinder. This mode can be termed S-IV, but it is different from the S-IV mode obtained by Khaledi *et al.*²¹ which was due to splitting of the vortices in the S-II mode. The spacing between the vortices is much smaller in this mode due to the high frequency forcing provided by the cylinder. Moreover, the vortex sizes are much smaller than those found in the S-II-I mode. Intuitively, we expect such high frequency modes to decay rapidly due to viscosity; thus, the effect of cylinder oscillation is felt in a narrow region in the downstream direction. It is therefore unsurprising that decreasing frequency ratio increases the extent of the discrete vortical structures as can be seen in Fig. 8(b) for $A/h = 0.3$ and $f_e/f_o = 4.5$. We therefore refer to this mode as S-IV-D, where S stands for symmetry, IV represents the four vortex pairs shed per cycle, and D stands for the vortex decay downstream.

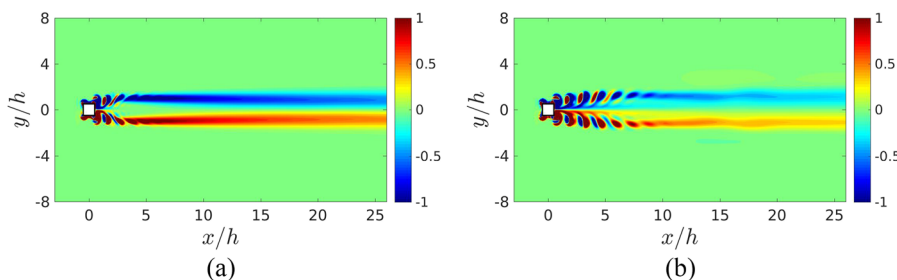


FIG. 8. S-IV-D symmetric mode obtained with (a) $A/h = 0.225$ and $f_e/f_o = 5.26$ and (b) $A/h = 0.3$ and $f_e/f_o = 4.5$. In our case, the cylinder center is at a distance of $8h$ from the inlet. (Color bars indicate vorticity in the z -direction in units of $1/s$.)

A movie attached in the [supplementary material](#) shows the evolution of vorticity contours over a few oscillation cycles.

1. Effect of frequency on S-IV-D mode

We report in [Fig. 5](#) that the vortex shedding is antisymmetric for $f_e/f_o < 3$. On increasing the frequency of excitation, two significant changes occur to the flow: one, the flow transitions to a symmetric mode near the cylinder, which we refer to as S-IV-D, and two, the dominant shedding frequency matches the excitation frequency. To understand how the S-IV-D mode emerges from an antisymmetric mode, we fix the amplitude ratio, A/h , at 0.225 and vary the frequency ratio, f_e/f_o , from 3.5 to 4.3. At $f_e/f_o = 3.5$ shown in [Fig. 9\(a\)](#), vortex shedding in the vicinity of the cylinder is symmetric even though it quickly disintegrates into an antisymmetric mode downstream. We refer to these intermediate modes with a small antisymmetric structure far downstream with the notation S-IV-D-A, where S-IV represents that the shedding in the

vicinity of the cylinder is an S-IV mode, D represents decay of vortical structures, and A stands for antisymmetric shedding occurring further downstream. The parameters at which these modes emerge are represented by the symbol (blue cross) in [Fig. 5](#). The symmetric region increases in length with frequency ratio until the entire pattern becomes symmetric, at least within the extent of the domain as shown in [Figs. 9\(b\)–9\(f\)](#). It is unclear at this stage if a true S-IV-D mode would appear if a domain of infinite downstream extent were to be used. To verify this fact, we plot the “length” of the symmetric region, l_s , with frequency ratio. Interestingly, the length follows a power law with frequency with a negative exponent as shown in [Fig. 10](#). A power-law fit of the form

$$l_s = l_0 (f_c^* - f_e^*)^{-\alpha} \quad (7)$$

appears to agree well with the numerical data. Here, the length l_0 is a numerical prefactor, $\alpha > 0$, f_c^* and f_e^* are the critical and

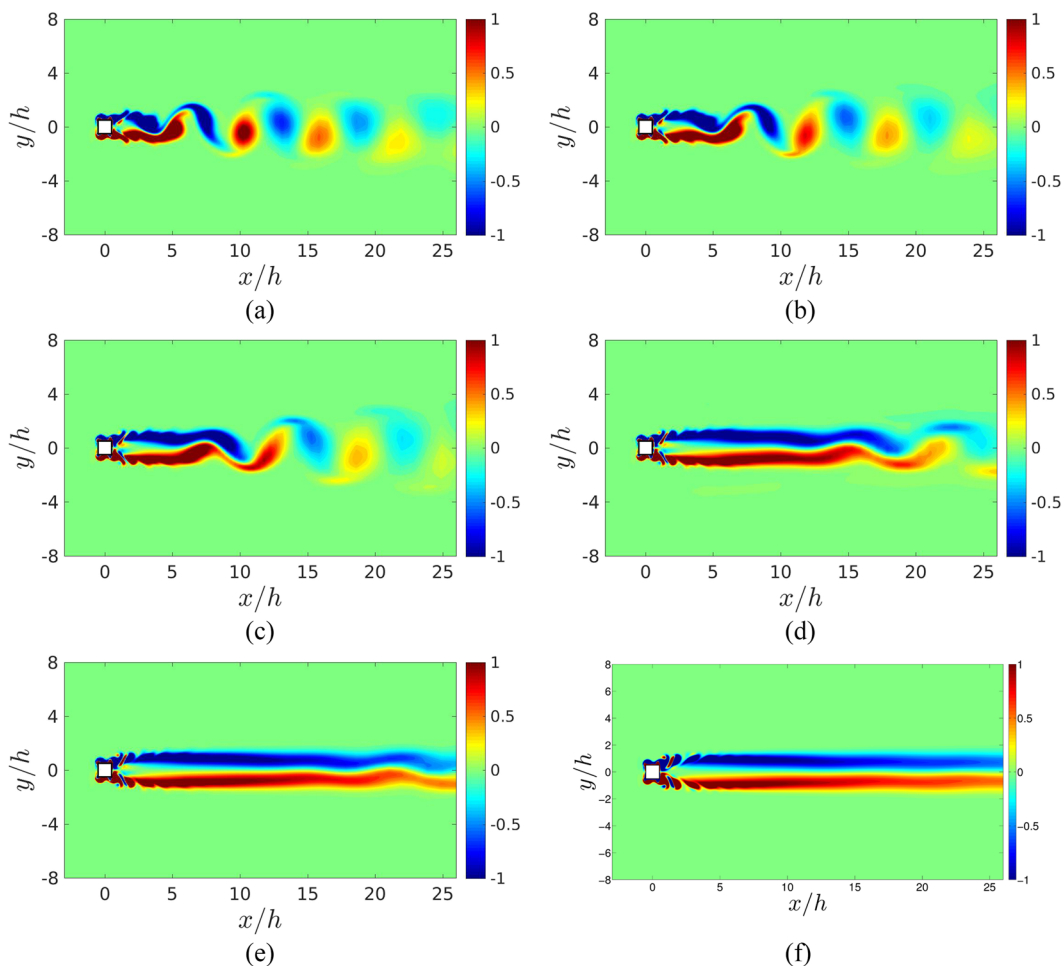


FIG. 9. Emergence of the symmetric mode S-IV-D with increasing frequency at a fixed $A/h = 0.225$: (a) $f_e/f_o = 3.5$, (b) $f_e/f_o = 3.7$, (c) $f_e/f_o = 3.9$, (d) $f_e/f_o = 4.1$, (e) $f_e/f_o = 4.2$, (f) $f_e/f_o = 4.3$. Because of an antisymmetric region downstream, we call these intermediate modes S-IV-D-A. In all cases, the cylinder center is at a distance of $8h$ from the inlet. (Color bars indicate vorticity in the z -direction in units of $1/s$.)

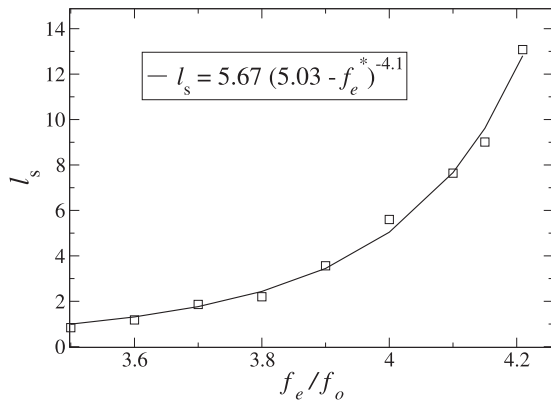


FIG. 10. Plot between the length at which first peak in vertical velocity reaches a value of 1% of U_m along the cylinder centerline from the cylinder center and frequency ratio (f_e/f_o).

excitation frequency normalized by the frequency f_o . We refer to f_e^* as the critical frequency as this is the frequency at which the length of symmetric region diverges, thus giving us a true symmetric S-IV-D mode even for a domain of infinite extent. Both f_e^* and α are determined by standard curve fitting techniques. The length of the symmetric region is determined as follows: we plot the vertical velocity along the centerline and take l_s to be equal to the length at which the vertical velocity reaches 1% of the mean inlet velocity. It has to be noted that for a perfectly symmetric mode, the vertical velocity, by symmetry, would be identically zero along the centerline. The exact length l_s from this procedure would therefore depend on the

cutoff % employed, thus l_0 is not a robust parameter. Nevertheless, the power-law dependence remains unaffected by the choice of the cutoff value for vertical velocity. It can therefore be stated with a high degree of certainty that a symmetric S-IV mode emerges for a nondimensional frequency ratio of 5.03 at this particular amplitude ratio.

C. Vortex flapping mode

A vortex flapping mode has been found in our simulation for $A/h \leq 0.5$ and $f_e \approx f_o$, represented by the symbol (open down-pointing triangle) in Fig. 5. The vorticity plot for $A/h = 0.4$ and $f_e/f_o = 0.8$ can be seen in Fig. 11(a). In this mode, the vortex street flaps about the centerline of the square cylinder over a time scale much longer than the shedding or excitation time scale. The entire evolution of the mode over one flapping time scale can be found in the supplementary material. A plot of the lift coefficient with time is shown in Fig. 12(a), and the corresponding frequency spectrum is shown in Fig. 12(b), which reveals distinct peaks. The frequency is normalized by inertial time scale, h/U_m . A dominant peak appears at f_o , which corresponds to the vortex shedding frequency, and a second peak appears at $|f_o - f_e|$, which is the frequency corresponding to the flapping time scale. Clearly, this mode shares strong similarities with the classical von Kármán street for a stationary cylinder with shedding at the same frequency as for a stationary cylinder. Using the numerical values of f_o and f_e , the nondimensional value of the flapping frequency is 0.03 for this particular case. This mode has been obtained previously by Krishnan *et al.*^{23,24} where they termed it as modulated wake. This mode seems similar to the beating string mode obtained by Detemple-Laake and Eckelmann⁹ where they obtained it by superimposing vortex shedding with sound waves. As $f_e \rightarrow f_o$, the flapping time scale becomes progressively longer, and at

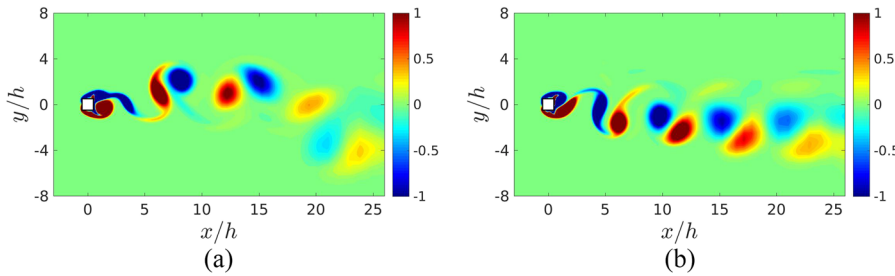


FIG. 11. (a) Vortex flapping mode obtained at $A/h = 0.4$ and $f_e/f_o = 0.8$ and (b) vortex shedding at an angle but with no flapping obtained at $A/h = 0.4$ and $f_e/f_o = 1$. In both cases, the cylinder center is at a distance of $8h$ from the inlet. (Color bars indicate vorticity in the z-direction in units of 1/s.)

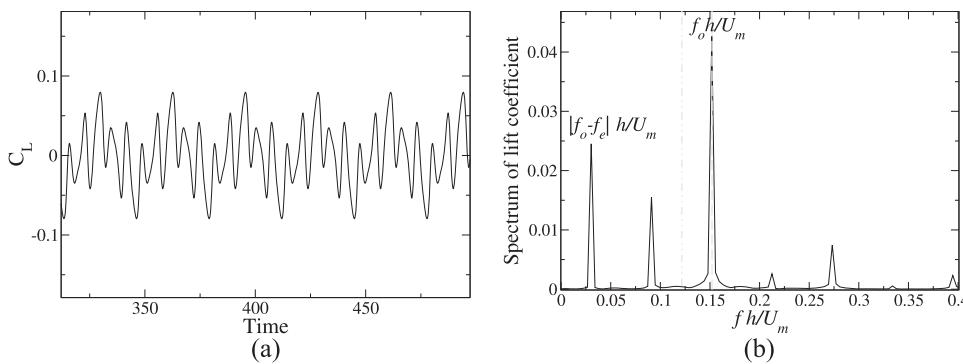


FIG. 12. (a) Variation in lift coefficient with time and (b) the spectrum of lift coefficient for $A/h = 0.4$ and $f_e/f_o = 0.8$ corresponding to the flapping mode of shedding.

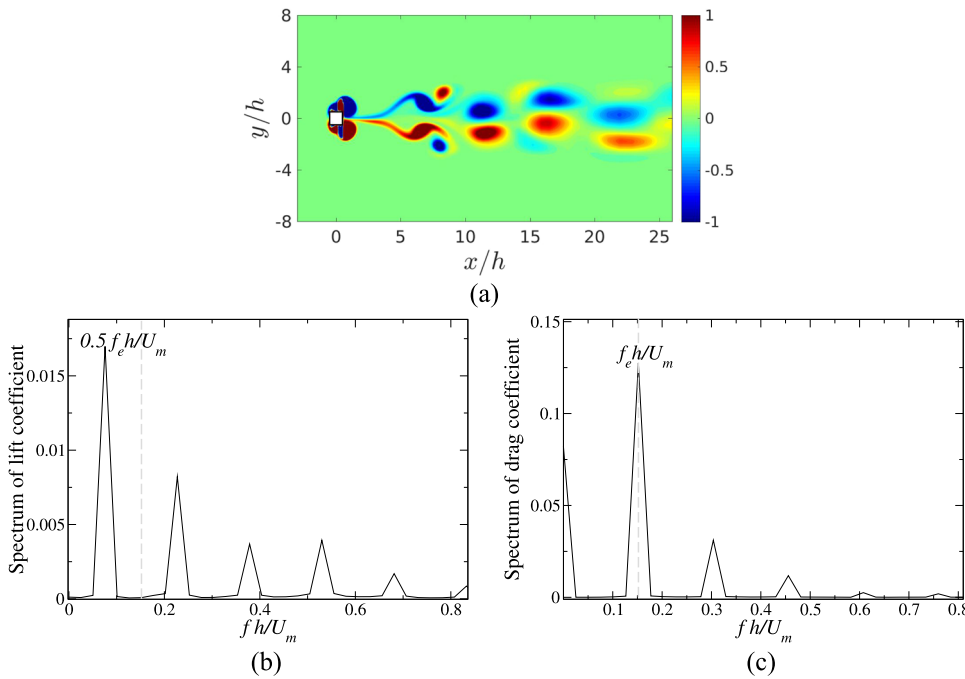


FIG. 13. (a) Vorticity contours for the S-II-A-II mode at $f_e/f_o = 1$ and $A/h = 0.7$ showing an S-II-like shedding in the vicinity of the cylinder and an antisymmetric arrangement of the dipoles further downstream, (b) the spectrum of lift coefficient, and (c) the spectrum of drag coefficient. In Fig. 13(a), the cylinder center is at a distance of $8h$ from the inlet. (Color bars indicate vorticity in the z -direction in units of $1/s$.)

$f_e/f_o = 1$, the flapping stops and the vortex street tilts to one side of the centerline as shown in Fig. 11(b). It has to be noted that the vortex street settling down on only one side of the centerline for $f_e \rightarrow f_o$ is dictated by factors such as the numerical scheme used for spatial and temporal discretization, preferential (but tiny) accumulation of numerical errors over the course of the numerical simulation, etc. The vortex shedding modes obtained in this region can be further classified as 2S (for two vortex shed in a cycle), 2P (for two pairs of

vortex shed in a cycle), or combination as has been done by Krishnan *et al.*²⁴

D. Vortex dipole mode (S-II-A-II)

We report a new mode of antisymmetric vortex shedding where alternate structures of vortex pairs or vortex dipoles arrange themselves in a zigzag pattern. This mode was represented by the

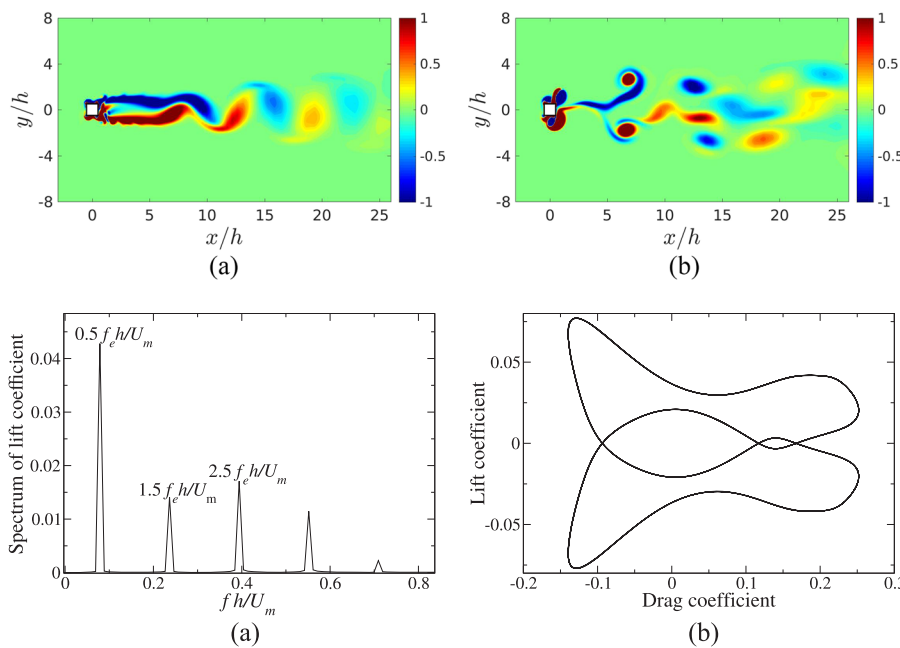


FIG. 14. Vorticity contours of ambiguous modes obtained with (a) $A/h = 0.2$ and $f_e/f_o = 4.5$, (b) $A/h = 0.875$ and $f_e/f_o = 1.0375$. (Color bars indicate vorticity in the z -direction in units of $1/s$.)

FIG. 15. Characteristics of ambiguous-II mode of Fig. 14(b): (a) the spectrum of lift coefficient, (b) the phase plot of lift vs drag coefficient showing that this is a nonchaotic mode.

symbol (green open left-pointing triangle) in Fig. 5, and the vorticity plot for $f_e/f_o = 1$ and $A/h = 0.7$ is shown in Fig. 13(a). In the vicinity of the cylinder, shedding resembles an S-II mode, but further downstream, these dipoles undergo rearrangement into an antisymmetric pattern. We therefore refer to this mode as S-II-A-II to represent an S-II mode in the vicinity of the cylinder and A-II mode, an alternating pattern of dipoles, further downstream. The spectrum of the drag and lift coefficients shown in Figs. 13(b) and 13(c) reveals that shedding is locked onto the excitation frequency f_e . We find only two instances of this mode occurring in our parametric study and is

perhaps the reason why this mode has not been reported in earlier studies. Physically, this mode appears to be driven by an instability caused to the S-I mode for $x/h > 10$.

E. Ambiguous mode

Apart from symmetric, antisymmetric, and chaotic modes, we find modes of vortex shedding which do not lend themselves to a clear classification. We therefore refer to these modes as “ambiguous” modes, which are represented by symbols (orange open

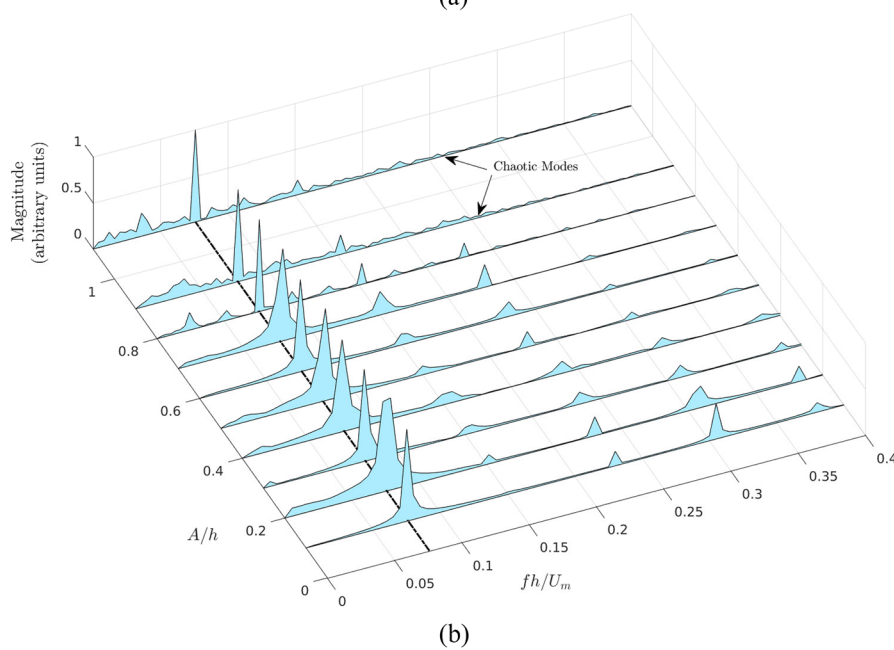
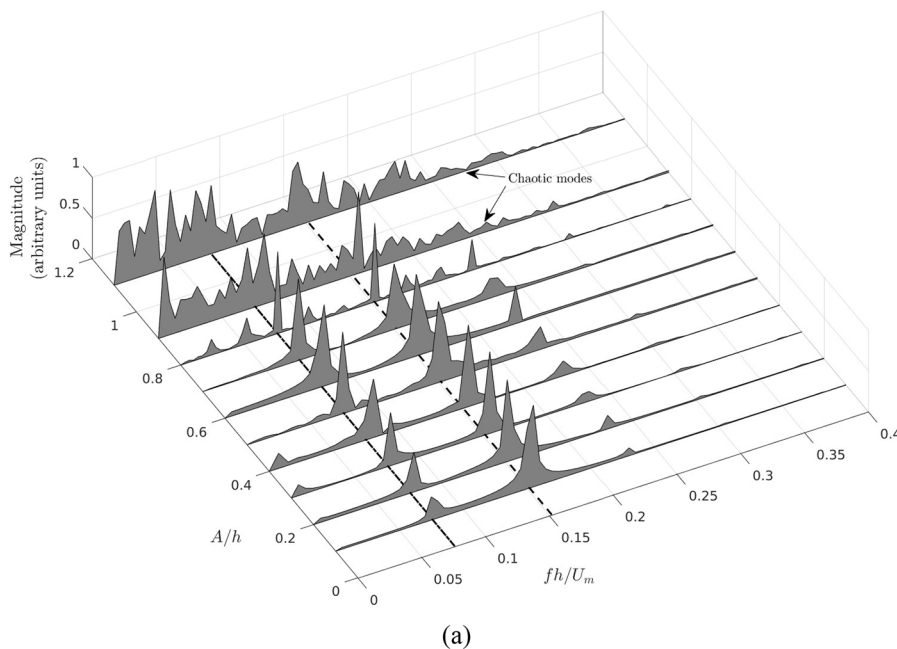


FIG. 16. Variation in the spectrum of lift coefficient (a) and drag coefficient (b) obtained at a fixed frequency ratio of $f_e/f_o = 0.5$ and varying the amplitude ratio A/h from 0.1 to 1.1.

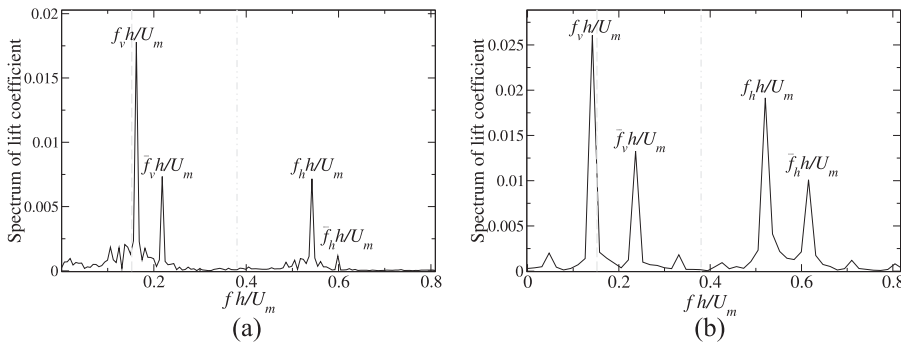


FIG. 17. Plot of the spectrum of lift coefficient obtained at (a) $A/h = 0.3$ and $f_e/f_o = 2.5$ and (b) $A/h = 0.4$ and $f_e/f_o = 2.5$.

up-pointing triangle) and (brown open right-pointing triangle) in Fig. 5.

Not surprisingly, the two types of ambiguous modes found in the present simulations occur in very different parts of the parametric space. The first ambiguous mode (Ambiguous-I) is found in the vicinity of $A/h = 0.2$ and $f_e/f_o = 4$, the location where S-IV modes are found in the parametric plot 5. The vorticity plot of this ambiguous mode at a particular time is shown in Fig. 14(a). This mode loosely resembles an S-IV mode in the near wake but with an antisymmetric character embedded within it. The mode clearly breaks down into an antisymmetric vortex pattern further downstream.

Another ambiguous mode (Ambiguous-II) is found in the vicinity of $f_e/f_o = 1.0375$ and $A/h = 0.875$. Vorticity contours for this mode, shown in Fig. 14(b), reveal a complex spatial arrangement of vortices, but this mode is clearly periodic as evident from the spectrum of lift coefficient and phase plot of lift vs drag coefficient in Fig. 15.

F. Effect of varying amplitude at a fixed excitation frequency

The region of superposition and lock-on found in the present simulations are in agreement with those found by Minewitsch *et al.*²⁸ Various dominant frequencies in the spectrum of lift coefficient reported by Minewitsch *et al.*²⁸ by varying amplitude ratio, A/h , at different frequency ratios, f_e/f_o , are also found in the present simulations. We decipher the role of amplitude of excitation on the frequency spectrum. We present results for three different frequency ratios, $f_e/f_o = 0.5$, $f_e/f_o = 2.5$, and $f_e/f_o = 4$. These frequency ratios cover a wide area in the parametric space of Fig. 5.

We first present the results for $f_e/f_o = 0.5$. Figure 16 shows the frequency spectrum of lift and drag coefficient at different amplitude ratios from $A/h = 0.1$ – 1.1 . For this frequency ratio, the ratio of the maximum body velocity to the inlet velocity increases from 0.0477 to 0.5254 as amplitude increases from 0.1 to 1.1. It can be seen from the frequency spectrum of lift coefficient that as the amplitude ratio increases, the strength of the peak at f_e progressively increases and eventually becomes comparable with the peak at f_o , the frequency of vortex shedding for a stationary cylinder, suggesting an eventual competition between natural frequency, f_o , of the unperturbed system and the external excitation frequency, f_e . It is therefore not surprising that the system becomes chaotic on further increase in the amplitude of oscillation as is commonly expected in most nonlinear oscillators when forced with an external excitation. The smaller peaks in the frequency spectrum are higher harmonics corresponding to $(f_o + f_e)$, $(f_o + 2f_e)$ and so on.

In the case of $f_e/f_o = 2.5$, Fig. 17(a) shows the spectrum of lift coefficient for two different amplitude ratios, $A/h = 0.3$ and 0.4 . Because of the higher forcing frequency, more frequencies emerge in the system. The dominant frequencies are f_v ($\approx f_o$), $f_h = |f_e + f_v|$, \tilde{f}_v ($\approx f_e/2$), and \tilde{f}_h ($= \tilde{f}_v + f_e$). Note that this frequency ratio is just beyond the window of lock-on shown in Fig. 3. If the systems were to be in a lock-on regime, then we expect f_v to be identically equal to $f_e/2$. We therefore see remnants of the lock-on frequency represented by \tilde{f}_v and \tilde{f}_h . This result is similar to that obtained by Minewitsch *et al.*²⁸ for $f_e/f_o = 2.4$ and $A/h = 0.35$. As the amplitude ratio is increased to 0.4, there is a significant increase in the influence of f_h and \tilde{f}_h and a minor increase in the influence of \tilde{f}_v as can be seen in Fig. 17(b). A further increase in excitation frequency to $f_e/f_o = 4$ at $A/h = 0.2$ reveals an abundance of combination frequencies such as

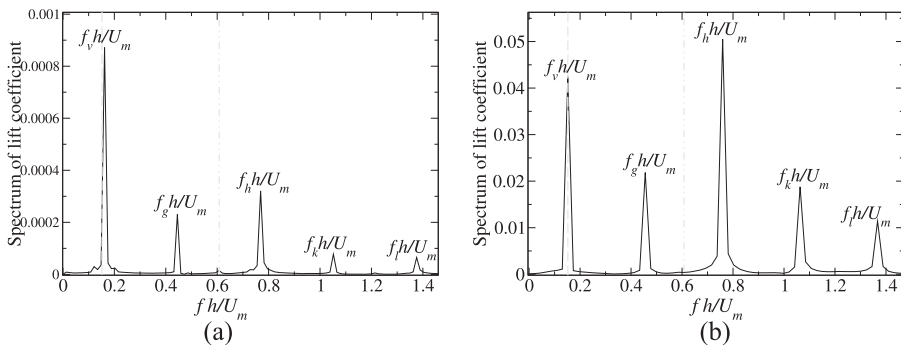


FIG. 18. Plot of the spectrum of lift coefficient obtained at (a) $A/h = 0.2$ and $f_e/f_o = 4$ and (b) $A/h = 0.3$ and $f_e/f_o = 4$.

$f_g = |f_e - f_o|$, $f_h = |f_e + f_o|$, $f_k = |2f_e - f_o|$, and $f_l = |2f_e + f_o|$ as shown in Fig. 18(a). A minor increase in amplitude ratio to 0.3 propels the dominance of f_h and other harmonics [Fig. 18(b)]. Similar results have been found for $f_e/f_o = 3, 4.5, \text{ and } 5$. In summary, an increase in amplitude promotes greater competition between the modes and eventually leads to chaotic regimes as shown in Fig. 5.

IV. CHAOTIC VORTEX SHEDDING

Several chaotic modes have been observed in our simulations and are represented by the symbol (open square) in Fig. 5. Each of these chaotic modes occur in different regions of the parametric space and are found to possess different frequency spectrum. We discuss just three representative cases in Fig. 19, one, in the large amplitude and small frequency range, two, in the small amplitude and large frequency range, and three, in a moderate amplitude and frequency range.

Figure 19(a) shows the phase portrait, with the lift coefficient plotted against the drag coefficient for $A/h = 1.125$ and $f_e/f_o = 1.026$.

A complex two lobed nonrepetitive structure is seen, which is indicative of a chaotic flow. The frequency spectrum of the lift coefficient shown in Fig. 19(b) shows a broadband spectrum but with a dominant peak near f_e or f_o shown by the dashed/dashed-dot vertical lines. Since this chaotic mode occurs in the vicinity of the S-II-I mode reported earlier (see Figs. 5 and 6), remnants of the dominant frequency of the S-II-I at frequency f_e are visible. Figure 19(c) shows the phase portrait for $A/h = 0.4$ and $f_e/f_o = 4$. This chaotic mode occurs in the vicinity of the S-IV-D modes discussed earlier, which themselves have a dominant peak at f_e . Therefore, the dominant peak in this chaotic mode is closer to f_e [Fig. 19(d)] with a sub-dominant peak occurring closer to f_o . The above two modes share one characteristic feature: they become chaotic when the strength of the forcing, determined by either a large amplitude or a large frequency, becomes comparable with the strength of the inlet flow. Therefore, these chaotic modes occur near the solid curved line in Fig. 5.

Chaos can also occur through a mode competition during the transition from antisymmetric to symmetric modes as discussed in

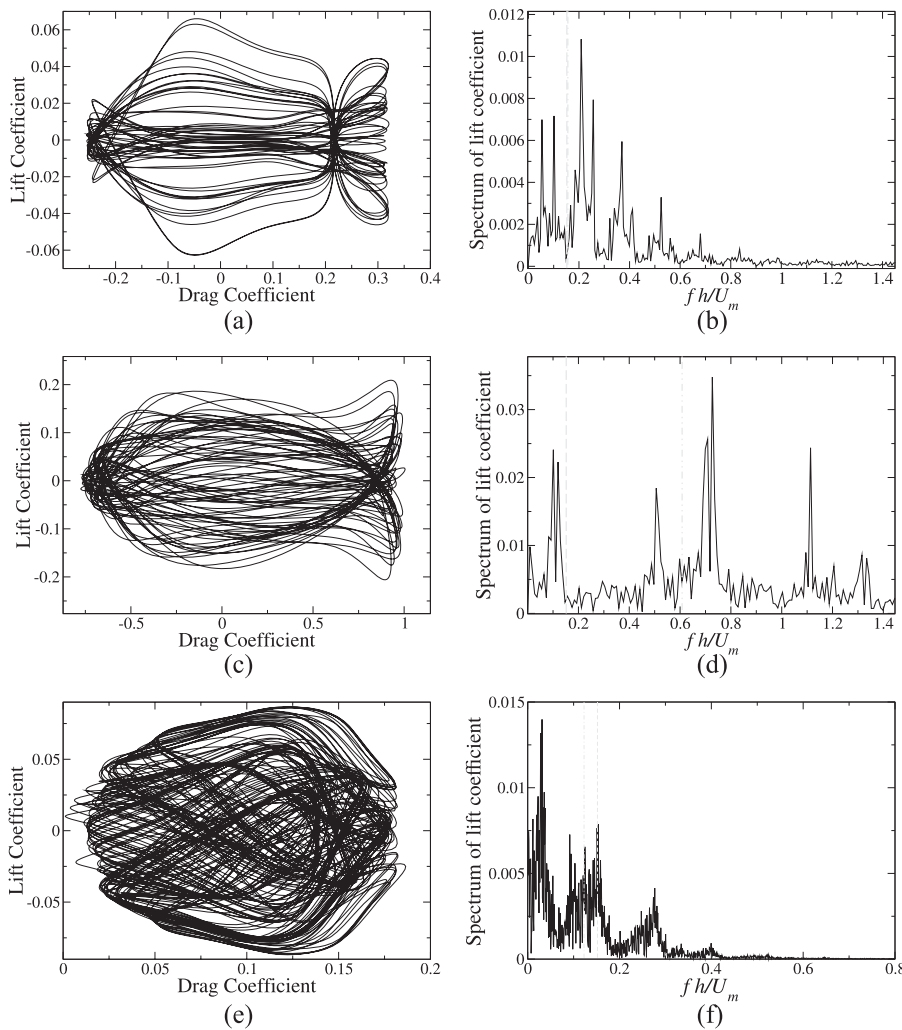


FIG. 19. Phase plot of lift vs drag coefficient (left panels) and frequency spectrum of lift coefficient (right panels) obtained at [(a) and (b)] $A/h = 1.125$ and $f_e/f_o = 1.026$, [(c) and (d)] $A/h = 0.4$ and $f_e/f_o = 4$, [(e) and (f)] $A/h = 0.54$ and $f_e/f_o = 0.807$.

Srikanth *et al.*³⁵ Such a competition occurs when the vortex flapping mode transitions to a S-II-I mode with increase in the amplitude of forcing. Figures 19(e) and 19(f) show the phase portrait and spectrum of lift coefficient at $A/h = 0.6$ and $f_e/f_o = 0.807$. The spectrum is dominated by the frequencies f_e and f_o as expected from modes which occur in the vicinity S-II-I mode and the flapping mode.

In the above discussion, chaos has been attributed to nonrepeating orbits in the phase plots or broadband spectrum in the frequency spectrum. Since this is an infinite-dimensional system, a more rigorous test for chaos is necessary. Determining the maximum Lyapunov exponent is difficult since phase-space representation is not possible from the available data. We therefore employ the 0-1 test for chaos proposed by Gottwald and Melbourne.^{16,17} The test has been validated for data obtained from logistic map and Lorenz equations before applying it to the time series data of lift coefficient. We only provide a brief discussion on this test and refer to the reader to Gottwald and Melbourne¹⁷ for a more complete discussion. For brevity, the results of chaos test for one single chaotic mode is presented below. Similar results were obtained for other chaotic modes.

Consider the discrete time series data of lift coefficient obtained from the numerical simulations to be represented by $C_L(t)$. These data are sampled at an optimal time interface, τ_{opt} , which is determined by the minimum of average mutual information curve. Mutual information method proposed by Fraser and Swinney¹⁴ has been found to be a useful way to generate coordinates for the reconstruction of strange attractor. In the present context, mutual information serves to determine if there is a temporal coherence in the time series data. We use the open source code developed by Weeks for determining the mutual information for the current data set.

We define a new variable, $L(t)$, which is the lift coefficient sampled discretely such that the time interval between successive recordings follows the relation $t_{i+1} - t_i = \tau_{opt}$. We now define translation variables as

$$p_c(n) = \sum_{j=1}^n L(j) \cos(jc), \quad q_c(n) = \sum_{j=1}^n L(j) \sin(jc) \quad (8)$$

for $n = 1, 2, \dots, N$ and $c \in (\pi/5, 4\pi/5)$. The mean square displacement of these translation variables can be computed for different values of c as follows:

$$M_c(n) = \lim_{N \rightarrow \infty} \frac{1}{N} \sum_{j=1}^N \left([p_c(j+n) - p_c(j)]^2 + [q_c(j+n) - q_c(j)]^2 \right), \quad (9)$$

where $n \ll N$. As suggested by Gottwald and Melbourne,¹⁷ ensuring that $n \leq n_{cut} = N/10$ was found to yield good results. The mean square displacement is indicative of the diffusive nature of the translation variables. If the dynamics is regular, then the mean square displacement is a bounded function in time and for chaotic dynamics, it scales linearly with time. A modified mean square displacement D_c can be defined to ensure better convergence properties but with the same asymptotic growth rate,

$$D_c(n) = M_c(n) - V_{osc}(n), \quad (10)$$

with

$$V_{osc}(c, n) = \langle E(L) \rangle^2 \left[\frac{1 - \cos nc}{1 - \cos c} \right]. \quad (11)$$

The expectation $\langle E(L) \rangle$ is given by

$$\langle E(L) \rangle = \lim_{N \rightarrow \infty} \frac{1}{N} \sum_{j=1}^N L(j). \quad (12)$$

With the modified mean square displacement, we can now compute the asymptotic growth rate K_c . We use the correlation method to calculate the correlation coefficient, K_c , which quantifies the correlation between $D_c(n)$ and linear growth. We define two vectors, $\xi = (1, 2, \dots, n_{cut})$ and $\Delta = (D_c(1), D_c(2), \dots, D_c(n_{cut}))$, and the correlation coefficient K_c given by

$$K_c = \text{corr}(\xi, \Delta) = \frac{\text{cov}(\xi, \Delta)}{\sqrt{\text{var}(\xi)\text{var}(\Delta)}} \in [-1, 1], \quad (13)$$

where the variance and covariance have their usual definitions. To ensure robustness of the measure to outliers and spurious resonances, the median value of K_c (say K) may be taken which is obtained for different random values of c . This value of K would lie close to 1 for chaotic signals and close to 0 for regular dynamics.

We apply the above 0-1 test for chaos for the chaotic signal observed at $f_e/f_o = 0.807$ and $A/h = 0.54$. Chaotic modes in this region, shown in Fig. 5, appear in a narrow window separating the antisymmetric vortex flapping modes and the symmetric S-II-I modes. It was predicted in earlier studies that a mode competition between symmetric and antisymmetric modes can occur at such boundaries. In the present study, it was found that this transition window is very narrow, with chaotic modes found at $A/h = 0.54$ and periodic modes on either side of it. The narrow window of chaos in this region also serves as a stricter case for the 0-1 test than other chaotic solutions reported in Fig. 5. We calculate K_c for two different amplitude ratios, at $A/h = 0.54$ and $A/h = 0.64$. The first case was found to be within the chaotic window, while the latter yielded a S-II-I periodic solution. Figure 20 shows a plot of K_c for different values of c . For $A/h = 0.54$, the median of K_c yields a

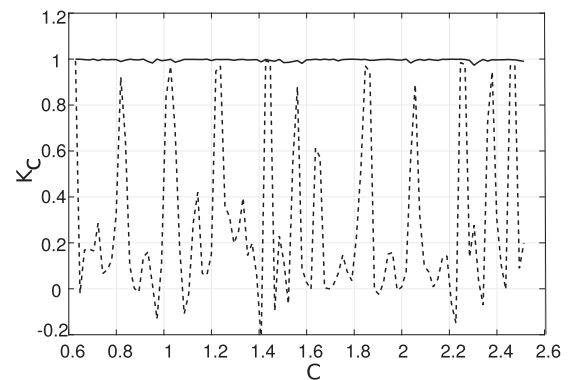


FIG. 20. Correlation coefficient K_c computed for lift coefficient time series with $f_e/f_o = 0.807$ and $A/h = 0.54$ (solid curve) and $A/h = 0.64$ (dashed curve).

value close to 1 (0.997 to be exact), while for $A/h = 0.64$, the median of K_c is close to 0 (0.145 to be exact). This conclusively shows that the time series for $f_e/f_o = 0.807$ and $A/h = 0.54$ indeed corresponds to a chaotic flow. Similar results were obtained for other chaotic cases.

V. COMPARISON WITH OSCILLATING CYLINDER EXPERIMENTS

In the previous sections, a detailed discussion was presented on how the shedding characteristics changed with varying amplitude and frequency of the cylinder. Here, we make a brief attempt at comparing the present simulation results with earlier experiments of Tatsuno and Bearman³⁶ for an oscillating circular cylinder in a quiescent flow. Such a comparison needs to be viewed with caution for two main reasons: (i) the shape of the cylinder is different in the two cases and (ii) the presence of large mean flow in the present simulations make the scenario very different from a quiescent flow case. Nevertheless, a comparison exercise could serve useful to compare and contrast the modes observed in the two types of studies.

Tatsuno and Bearman³⁶ carried out an extensive visual study of a circular cylinder in a quiescent flow. They observed a number of modes with varying Keulegan-Carpenter, $KC \in (0, 15)$, and Stokes, $\beta \in (0, 160)$, numbers. For comparison, we have indicated the KC and β ranges in our present study in Fig. 5. It has to be noted that any qualitative similarity with experiments should be construed as indicative rather than conclusive and may not necessarily occur in the same parameter range in the present study. Tatsuno and Bearman classified their modes as A^*-G . The mode A^* was observed for low KC at almost all values of β , and this mode corresponds to emergence of tiny symmetric vortices on either side of the cylinder but without any vortex shedding. Therefore, the addition of a large mean flow like in the present study is expected to remain insensitive to small oscillations induced by the cylinder. Hence, in a similar parameter range, we observe Kármán or near-Kármán type vortex shedding.

In regime A which was observed only for $\beta < 50$, stronger symmetric vortices emerge on either side of the cylinder which begin to shed for larger values of KC . With a mean flow, the resultant vortex shedding pattern is expected to be a combination of vortex pattern without cylinder oscillations and the symmetric pattern observed in regime A. In the present study, regime A partly overlaps with symmetric shedding mode S-II-I. This is suggestive of significant interaction between the symmetric modes of regime A with the natural vortex shedding mode for a stationary cylinder.

There is no analogue of regime B in the present study since Tatsuno and Bearman noted this to be a fully 3D mode. It was pointed out by Elston *et al.*¹¹ that this regime can be explained with a Floquet analysis as a secondary instability on the two-dimensional base state. We observe symmetric shedding modes S-IV in this parameter space.

Regimes D and E are peculiar and correspond to asymmetric vortex shedding. In regime D, Tatsuno and Bearman noted that vortex shedding tilted to one side of the oscillating cylinder, whereas in regime E, aperiodic changes to the direction of shedding occurred. Such symmetric breaking modes are also observed in the present study and have been termed either vortex flapping modes or chaotic

modes. But the flapping modes were observed for much lower values of KC than those corresponding to regime D. Chaotic modes were not reported in Tatsuno and Bearman. It has to be noted that the mode-competition route to chaos is completely absent in their experiment.

VI. CONCLUSIONS

In this work, a systematic study of vortex shedding past an inline oscillating square cylinder at a Reynolds number of 200 is presented. The amplitude of cylinder oscillation and the frequency of excitation were varied, spanning over 100 computer simulations, to reveal a number of new features. Some of these features, such as the observation of two new symmetric modes, a fully stable S-II-I mode and S-IV-D modes, and the vortex dipole mode, S-II-A-II, are being reported for the first time, while other features such as vortex flapping modes and chaotic modes have been investigated in greater detail. A summary of all simulations, shown in Fig. 5, shows clustering of modes based on the structure of the vortex street.

In the S-II-I mode of Fig. 6, two pairs of vortices are shed for every cycle of cylinder oscillation symmetrically, of which the secondary pair gets sheared away downstream. This results in a stable S-I mode downstream of the cylinder. This mode is found in the top-left region of the parameter space of Fig. 5 which corresponds to moderate/large values of amplitude ratio and small frequency ratio. In the bottom-right region of the parameter space of Fig. 5 which corresponds to low values of amplitude ratio but high values of frequency ratio, we find another symmetric mode which we name S-IV-D. This mode is characterized by two pairs of vortex dipoles shed on each side of the cylinder in every cycle of cylinder oscillation. A systematic study of these symmetric modes is presented in this paper. In addition, we also study the emergence of the S-IV-D mode from an antisymmetric state as a function of the frequency. We find that the length of the symmetric region increases with frequency and obeys a power law with a negative exponent. This suggests that a true S-IV-D mode (even in a domain of infinite length) emerges when the frequency reaches a critical value.

Another interesting feature observed in the present simulations is the emergence of the so-called “flapping mode” where the entire vortex street oscillates about the centerline. This mode is characterized by two time scales, a fast time scale at frequency f_o corresponding to the shedding of individual vortices from the cylinder and a slow time scale at frequency $|f_o - f_e|$ corresponding to the flapping frequency. As $f_e \rightarrow f_o$, the time scale of flapping which is proportional to $1/|f_e - f_o|$ becomes progressively longer and eventually leads to an oblique shedding when $f_e = f_o$. We also find a range of new combination frequencies such as $f_h = |f_v + f_e|$, $f_g = |f_e - f_o|$, $f_k = |2f_e - f_o|$, and $f_l = |2f_e + f_o|$ appear with the increase in either amplitude or frequency of excitation. Interactions between these new frequencies often leads to chaos. We find that such chaos usually occurs when the cylinder velocity ($A \times 2\pi f_e$) becomes comparable with the inlet velocity, U_m , as shown by the solid curved line in Fig. 5. Another route to chaos observed in our analysis is a mode-competition mechanism during the transition from an antisymmetric shedding to a symmetric shedding.

A number of issues remain unexplored and are briefly discussed below. Some of these questions are currently being addressed and will be presented elsewhere. A systematic bifurcation diagram for the

transition to chaos when shedding transforms from antisymmetric to symmetric type is unknown. The evolution of the different modes obtained in this paper by varying the two parameters (amplitude ratio and frequency ratio) is currently being studied with the help of linear stability analysis. It is well known that the antisymmetric pattern found in the classical von Kármán vortex street can be predicted using a local stability analysis on a stationary wake profile (see Hultgren and Agarwal²⁰). We are attempting a similar analysis on an oscillating velocity profile. Another avenue of interest is to understand the energetics of such wake flows with emphasis on transfer of energy between the mean and oscillatory fields.¹⁰

SUPPLEMENTARY MATERIAL

For animations of S-II-I mode presented in Sec. III A and vortex flapping model presented in Sec. III C, see [supplementary material](#) online.

ACKNOWLEDGMENTS

This work was carried out as part of graduate studies of the first author at IIT Hyderabad. H.S.R. thanks the Ministry of Human Resource Development, Government of India, for funding his graduate studies, and H.N.D. thanks IIT Hyderabad for financial support. We also thank Professor Eric Weeks (Emory University) for freely making his mutual information code available on his website.

REFERENCES

- E. M. Alawadhi, "Numerical simulation of fluid flow past an oscillating triangular cylinder in a channel," *J. Fluids Eng.* **135**, 041202 (2013).
- E. M. Alawadhi, "Numerical simulation of flow past an elliptical cylinder undergoing rotationally oscillating motion," *J. Fluids Eng.* **137**, 031106 (2015).
- S. Ansumali, S. S. Chikatamarla, C. E. Frouzakis, and K. Boulouchos, "Entropic lattice Boltzmann simulation of the flow past square cylinder," *Int. J. Mod. Phys. C* **15**(3), 435 (2004).
- C. Barbi, D. P. Favier, C. A. Maresca, and D. P. Telionis, "Vortex shedding and lock-on of a circular cylinder in oscillatory flow," *J. Fluid Mech.* **170**, 527 (1986).
- H. M. Blackburn and R. D. Henderson, "A study of two-dimensional flow past an oscillating cylinder," *J. Fluid Mech.* **385**, 255–286 (1999).
- M. K. Chauhan, S. Dutta, B. K. Gandhi, and B. S. More, "Experimental investigation of flow over a transversely oscillating square cylinder at intermediate Reynolds number," *J. Fluids Eng.* **138**, 051105 (2016).
- G.-H. Cottet and P. D. Koumoutsakos, *Vortex Methods: Theory and Practice* (Cambridge University Press, 2000).
- Y. Couder and C. Basdevant, "Experimental and numerical study of vortex couples in two-dimensional flows," *J. Fluid Mech.* **173**, 225–251 (1986).
- E. Detemple-Laake and H. Eckelmann, "Phenomenology of Kármán vortex streets in oscillatory flow," *Exp. Fluids* **7**, 217 (1989).
- S. S. Dol, M. M. Salek, and R. J. Martinuzzi, "Energy redistribution between the mean and pulsating flow field in a separated flow region," *J. Fluids Eng.* **136**, 111105 (2014).
- J. R. Elston, H. M. Blackburn, and J. Sheridan, "The primary and secondary instabilities of flow generated by an oscillating circular cylinder," *J. Fluid Mech.* **550**, 359–389 (2006).
- J. R. Elston, J. Sheridan, and H. M. Blackburn, "Two-dimensional Floquet stability analysis of the flow produced by an oscillating circular cylinder in quiescent fluid," *Eur. J. Mech.: B/Fluids* **23**, 99–106 (2004).
- A. Feynmark, N. Alin, R. Bensow, and C. Fureby, "Numerical simulation of an oscillating cylinder using large eddy simulation and implicit large eddy simulation," *J. Fluids Eng.* **134**, 031205 (2012).
- A. M. Fraser and H. L. Swinney, "Independent coordinates for strange attractors from mutual information," *Phys. Rev. A* **33**, 1134–1140 (1986).
- F. A. González, M. A. Cruchaga, and D. J. Celentano, "Analysis of flow past oscillatory cylinders using a finite element fixed mesh formulation," *J. Fluids Eng.* **139**, 081202 (2017).
- G. A. Gottwald and I. Melbourne, "A new test for chaos in deterministic systems," *Proc. R. Soc. London, Ser. A* **460**, 603–611 (2004).
- G. A. Gottwald and I. Melbourne, "On the implementation of the 0-1 test for chaos," *SIAM J. Appl. Math.* **8**, 129–145 (2009).
- O. M. Griffin and M. S. Hall, "Vortex shedding lock-on and flow control in bluff body wakes," *J. Fluids Eng.* **113**, 526–537 (1991).
- O. N. Griffin and S. E. Ramberg, "Vortex shedding from a cylinder vibrating in line with an incident uniform flow," *J. Fluid Mech.* **75**, 257 (1976).
- L. S. Hultgren and A. K. Aggarwal, "Absolute instability of the Gaussian wake profile," *Phys. Fluids* **30**, 3383–3387 (1987).
- H. A. Khaledi, H. I. Andersson, M. Barri, and B. Pettersen, "Flow past a normal flat plate undergoing inline oscillations," *Phys. Fluids* **24**, 093603 (2012).
- E. Konstantinidis and S. Balabani, "Symmetric vortex shedding in the near wake of a circular cylinder due to streamwise perturbations," *J. Fluids Struct.* **23**, 1047 (2007).
- H. Krishnan, A. Agrawal, A. Sharma, M. Thompson, and J. Sheridan, "Characteristics of force coefficients and energy transfer for vortex shedding modes of a square cylinder subjected to inline excitation," *J. Fluids Struct.* **81**, 270–288 (2018).
- H. Krishnan, A. Amit, A. Sharma, and J. Sheridan, "Near-body vorticity dynamics of a square cylinder subjected to an inline pulsatile free stream flow," *Phys. Fluids* **28**(9), 093605 (2016).
- S. Kumar, "Effect of channel inlet blockage on the wake structure of a rotationally oscillating cylinder," *J. Fluids Eng.* **138**, 121203 (2016).
- Y. Lecoq and J. Piquet, "Flow structure in the wake of an oscillating cylinder," *J. Fluids Eng.* **111**, 139–148 (1989).
- S. B. Lee, "Response of a circular cylinder wake to periodic wave excitations," *J. Fluids Eng.* **140**, 061202 (2018).
- S. Minewitsch, R. Franke, and W. Rodi, "Numerical investigation of laminar vortex-shedding flow past a square cylinder oscillating in line with the mean flow," *J. Fluids Struct.* **8**, 787 (1994).
- N. Nabatian, X. Xu, and N. Mureithi, "POD analysis of three-dimensional harmonically forced wake flow of a circular cylinder," *Trans. Can. Soc. Mech. Eng.* **39**(4), 789–803 (2015).
- A. Okajima, "Strouhal numbers of rectangular cylinders," *J. Fluid Mech.* **123**, 379 (1982).
- A. Ongoren and D. Rockwell, "Flow structure from an oscillating cylinder Part 2. Mode competition in the near wake," *J. Fluid Mech.* **191**, 225 (1988).
- P. G. Perdikaris, L. Kaiktsis, and G. S. Triantafyllou, "Chaos in a cylinder wake due to forcing at the Strouhal frequency," *Phys. Fluids* **21**, 101705 (2009).
- S. Peter and A. K. De, "Characteristics of the wake behind a transversely oscillating cylinder near a wall," *J. Fluids Eng.* **139**, 031201 (2017).
- A. Sohankar, C. Norberg, and L. Davidson, "Numerical simulation of unsteady low-Reynolds number flow around rectangular cylinders at incidence," *J. Wind Eng. Ind. Aerodyn.* **69-71**, 189–201 (1997).
- T. Srikanth, H. N. Dixit, T. Rao, and R. Govindarajan, "Vortex shedding patterns, their competition, and chaos in flow past inline oscillating rectangular cylinders," *Phys. Fluids* **23**, 073603-1–073603-9 (2011).
- M. Tatsuno and P. W. Bearman, "A visual study of the flow around an oscillating circular cylinder at low Keulegan-Carpenter numbers and low Stokes numbers," *J. Fluid Mech.* **211**, 157–182 (1990).
- G. H. Toebe, "The unsteady flow and wake near an oscillating cylinder," *J. Basic Eng.* **91**, 493–505 (1969).
- G. Vittori and P. Blondeaux, "Quasiperiodicity and phase locking route to chaos in 2-D oscillatory flow around a circular cylinder," *Phys. Fluids A* **5**(8), 1866 (1993).
- H. G. Weller, G. Tabor, H. Jasak, and C. Fureby, "A tensorial approach to computational continuum mechanics using object-oriented techniques," *Comput. Phys.* **12**(6), 620–631 (1998).

⁴⁰C. H. K. Williamson and R. Govardhan, "Vortex-induced vibrations," *Annu. Rev. Fluid Mech.* **36**, 413–455 (2004).

⁴¹S. J. Xu, Y. Zhou, and M. H. Wang, "A symmetric binary-vortex street behind a longitudinally oscillating cylinder," *J. Fluid Mech.* **556**, 27 (2006).

⁴²Y. Zhang and K. Zhu, "Flow over an inline oscillating circular cylinder in the wake of a stationary circular cylinder," *Fluid Dyn. Res.* **49**, 015504 (2016).

⁴³C. Y. Zhou and J. M. R. Graham, "A numerical study of cylinders in waves and currents," *J. Fluids Struct.* **14**, 403 (2000).